AFOSR-TR- 88-0970

SC5459.AR

Copy No. 4

PROCESSABILITY AND HIGH TEMPERATURE BEHAVIOR OF EMERGING AEROSPACE ALLOYS

ANNUAL REPORT NO. 2 FOR THE PERIOD May 01, 1987 through April 30, 1988

CONTRACT NO. F49620-86-C-0058

Prepared for

Air Force Office of Scientific Research
Directorate of Electronic and Material Sciences
Building 410
Bolling AFB, DC 20332-6448

Part I: A.K. Ghosh
Part II: C.G. Rhodes
Principal Investigators

AUGUST 1988

Rockwell International
Science Center

UNCLASSIFIED

SECURITY CLASSIFICATION OF THIS PAGE

REPORT DOCUMENTATION PAGE

FORM APPROVED OMB No. 0704-0188

1a. REPORT SECURITY CLASSIFICATION
UNCLASSIFIED

1b. RESTRICTIVE MARKINGS

2a. SECURITY CLASSIFICATION AUTHORITY

2b. CLASSIFICATION/DOWNGRADING SCHEDULE

3. DISTRIBUTION/AVAILABILITY OF REPORT
Approved for public release; distribution unlimited

4. PERFORMING ORGANIZATION REPORT NUMBER(S)
SC5459.AR

5. MONITORING ORGANIZATION REPORT NUMBER(S)
AFOSR-TR 88-0970

6a. NAME OF PERFORMING ORGANIZATION
ROCKWELL INTERNATIONAL Science Center

6b. OFFICE SYMBOL (If Applicable)

7a. NAME OF MONITORING ORGANIZATION
AFOSR/NE

6c. ADDRESS (City, State, and ZIP Code)
1049 Camino Dos Rios Thousand Oaks, CA 91360

7b. ADDRESS (City, State and ZIP Code)
Bldg 410 Bolling AFB, DC 20332

8a. NAME OF FUNDING/SPONSORING ORGANIZATION
Air Force Office of Scientific Research

8b. OFFICE SYMBOL (If Applicable)
NE

9. PROCUREMENT INSTRUMENT IDENTIFICATION NUMBER
CONTRACT NO. F49620-86-C-0058

8c. ADDRESS (City, State and ZIP Code)
Building 410 Bolling AFB, DC 20332

10. SOURCE OF FUNDING NOS.

PROGRAM ELEMENT NO.	PROJECT NO.	TASK NO.	WORK UNIT ACCESSION NO.
61102F	2306/A1	A1	

11. TITLE (Include Security Classification)
PROCESSABILITY AND HIGH TEMPERATURE BEHAVIOR OF EMERGING AEROSPACE ALLOYS (U)

12. PERSONAL AUTHOR(S)
Ghosh, A.K. and Rhodes, C.G.

13a. TYPE OF REPORT	13b. TIME COVERED	14. DATE OF REPORT (Year, Month, Day)	15. PAGE COUNT
Annual Report	FROM **05/01/87** TO **04/30/88**	**1988, AUGUST**	

16. SUPPLEMENTARY NOTATION

17. COSATI CODES			18. SUBJECT TERMS (Continue on reverse if necessary and identify by block number)
FIELD	GROUP	SUB-GROUP	

19. ABSTRACT (Continue on reverse if necessary and identify by block number)

This annual report describes progress during the second year of the three year research program to study the relationship between processing, microstructure and properties of advanced aerospace alloys.

Part I of this program examines a unified approach for understanding and assessing microstructure changes under the influence of different modes of thermomechanical and deformation processing. Experimental validation of the microstructure changes occurring in advanced aluminum alloys, such as SiC particulate reinforced aluminum, high strength P/M aluminum and high temperature aluminum alloy, Al-8Fe-4Ce, are being conducted. Progress of microstructural refinement and changes in misorientation between subgrains are determined to delineate the path for optimum processability for these alloys. The effects of various processing conditions on texture and elevated temperature deformation characteristics have been studied.

20. DISTRIBUTION/AVAILABILITY OF ABSTRACT
UNCLASSIFIED/UNLIMITED ☐ SAME AS RPT. ☒ DTIC USERS ☐

21. ABSTRACT SECURITY CLASSIFICATION
UNCLASSIFIED

22a. NAME OF RESPONSIBLE INDIVIDUAL
Rosenstein

22b. TELEPHONE NUMBER (Include Area Code)
(202) 767-4933

22c. OFFICE SYMBOL
NE

DD FORM 1473, JUN 86 Previous editions are obsolete.

UNCLASSIFIED

SECURITY CLASSIFICATION OF THIS PAGE

Part II of the program is a study of the effects of Fe, C, O, and Si as minor additions and Nb and V as major additions to Ti-22Al-8Nb on 675°C creep behavior. The results have demonstrated that the effects of the individual additives on creep resistance for the Ti_3Al base alloy are essentially the same as those previously observed for conventional titanium alloys. Si and Si + Zr are effective for improving creep resistance of the alpha-two alloys by pinning mobile dislocations during creep exposure. Close control of iron to its lowest possible level is also an effective approach to increased creep resistance. Carbon additions enhance creep resistance as well, albeit to a lesser extent than silicon. Primary creep behavior as a function of alloying addition follows the same general trend as the minimum creep rate.

TABLE OF CONTENTS

LIST OF FIGURES

LIST OF FIGURES

LIST OF TABLES

1.0 ABSTRACT

This annual report describes progress during the second year of the three-year research program to study the relationship between processing, microstructure and properties of advanced aerospace alloys.

Part I of this program examines a unified approach for understanding and assessing microstructural changes under the influence of different modes of thermomechanical and deformation processing. Experimental validation of the microstructural changes occurring in advanced aluminum alloys, such as SiC particulate-reinforced Al, high-strength P/M Al and high-temperature Al alloy, Al-8Fe-4Ce, are being conducted. Progress of microstructural refinement and changes in misorientation between subgrains are determined to delineate the path for optimum processability for these alloys. The effects of various processing conditions on texture and elevated temperature deformation characteristics have been studied.

Part II of the program is a study of the effects of Fe, carbon, oxygen and Si as minor additions, and Nb and V as major additions to Ti-22Al-8Nb on 675°C creep behavior. The results have demonstrated that the effects of the individual additives on creep resistance for the Ti_3Al base alloy are essentially the same as those previously observed for conventional Ti alloys. Si and Si + Zr are effective for improving creep resistance of the α_2 alloys by pinning mobile dislocations during creep exposure. Close control of Fe to its lowest possible level is also an effective approach to increased creep resistance. Carbon additions enhance creep resistance as well, although to a lesser extent than Si. Primary creep behavior as a function of alloy addition follows the same general trend as the minimum creep rate.

2.0 INTRODUCTION

Processing, properties and microstructure form a close interrelationship determining the structural performance of metallic materials. Microstructure and alloy composition not only determine properties that are important for structural performance, but properties that control the processability of structural alloys. In turn, the processing methods used to fabricate components, e.g., forging or forming operations, and the microstructure resulting from them dictate structural performance. This two-part research program is designed to investigate two aspects of airframe material processing. In Part I, microstructural control and processability in Al alloys is being investigated, and the effect of microstructural conditions on widening the processing windows within which material could be successfully processed is being determined. In Part II, the creep behavior of high-temperature titanium aluminide alloys is being examined, and the importance of alloy additives on the mechanisms of creep will be determined.

Modern metallic materials for aerospace applications are becoming increasingly complex in character. With rapidly solidified high-strength and high-temperature materials on one hand and the emergence of low-density Al-Li alloy on the other, the development of new Al alloys is preceding the development of cost-effective processing technologies such as superplastic forming, isothermal forging and other hot-working operations. The significant impact of processing on microstructure and properties cannot be overestimated, particularly in the development of these new Al alloys where microstructural instability could lead to degradation in properties. It is being realized that empirical approaches to shaping of these alloys must be replaced by an overall approach to improving processability, which is based on the understanding of the micromechanics and is extrapolatable from one type of shape change to another. This subject is examined in Part I with the objective of developing a science base for providing a unified approach which is applicable to different processing modes. This involves appropriate microstructural control using processes of dynamic recovery and static recrystallizations, and strain-induced grain boundary migration.

Specific experimental approaches have focused on two advanced Al base materials: particulate SiC-reinforced Al sheets and high-temperature Al alloy, Al-8Fe-4Ce. Microstructural changes during deformation processing along a variety of strain paths are being determined. Such changes involve quantitative characterization of grain (or sub-

grain) size and misorientations as a function of processing history. In addition, the distribution of particulate reinforcements is monitored as a function of strain.

A method of three-axis forging has been devised, in which a block of metal is compressed under plane strain conditions to a high level of strain, and then rotated between successive passes to impart a very large level of strain without an overall change in the shape or size of the block. By adjusting the deformation temperature to allow dynamic recovery (not recrystallization), an extremely fine-grain microstructure could be produced. The effect of this deformation mode, which involves shear along three orthogonal directions on the microstructural features, is investigated.

Part II of this program addresses creep behavior in high-temperature intermetallics designed for aerospace applications. The performance requirements of skins and subsurface structural components which will be exposed to exceptionally high temperatures in hypersonic and transatmospheric vehicles are of considerable current concern. The development of high thrust-to-weight ratio turbine engines for these advanced aircraft has also provided impetus for significant activity aimed at developing lightweight, elevated temperature materials. An alloy system emerging as a prime candidate for turbine engine applications is one based on the intermetallic compound Ti_3Al.

First-tier properties, such as tensile strength and ductility, have been well documented on alloys designated as potential structural materials. As particular alloy compositions evolve for high-temperature applications, second-tier properties, such as creep resistance, need to be evaluated.

This program is designed to examine elevated temperature creep behavior of Ti_3Al base alloys. There is an established literature base on the effects of minor alloying additions on the creep behavior of conventional Ti alloys. That base was used to compose alloy chemistries for study in this program. The effects of minor additions on both steady-state creep rate and primary creep strain will be assessed.

3.0 PROGRESS

3.1 Summary of Progress

During the second year of this research program, progress has been made on Parts I and II. The results are summarized below.

The development of optimum processing schemes for advanced Al alloys requires a thorough understanding of the process of microstructural changes occurring during thermomechanical and deformation processing steps, and their relationship to the flow characteristics of these alloys. With the aim of developing a unified approach toward this goal, a combined experimental and theoretical investigation was initiated in Part I. Earlier, a model of subgrain creep has been developed which ties the microstructural size and misorientation between subgrains occurring during deformation with stress and strain levels applied. Experiments are being conducted with three different advanced Al alloys: 1) a high-strength RST Al alloy (7064); 2) a SiC particulate-reinforced Al alloy of the same composition and processing; and 3) a high-temperature Al alloy, Al-8Fe-4Ce. These alloys have been thermomechanically processed by a variety of deformation methods, including compression, thermal cycling, torsion and three-axis multistep forging. Microstructures developed show extreme fineness to levels of 0.5-1.5 μm. Furthermore, the misorientations between grains (or subgrains) have been found to increase continuously with increasing accumulated strain levels up to 12-14. Crystallographic texture measurements show that extruded and three-axis forged materials are unrecrystallized, which can be recrystallized by heavy rolling passes. Optimum temperature and strain-rate windows for processing these materials have also been developed, which arise in part from postponement of necking due to strain-hardening effects.

In Part II of the program, the effects of minor alloying additions to Ti-22Al-8Nb (at.pct.) on 675°C creep behavior have been examined. During this second year, detailed analyses of Phase I creep test samples have been conducted. Quantitative correlations of steady-state creep rates with alloying additives were made, along with TEM analyses of dislocation character. It was demonstrated that Fe additions have the most significant (negative) effect on secondary creep rates, when compared to C or Si additions at levels of less that 0.2 at% (0.12 wt%). There is evidence that Fe reduces creep resistance by promoting addition slip system activation. The increase in creep

resistance due to carbon has been attributed to solid solution strengthening of the DO_{19} matrix. On the other hand, Si improves creep resistance by means of a dislocation pinning mechanism. Seven alloys have been selected for study in Part I, Phase II, having the base composition of Ti-24Al-11Nb (at.pct.) with systematic additions of Fe, C and Si.

3.2 Part I. Microstructural Control and Processability in Al Alloys

This section describes the progress made on Part I during the second year of the three-year program relating microstructural development with deformation processing, and the development of optimum processing schemes for advanced Al alloys.

3.2.1 Background

Modern Al alloys for aerospace applications are becoming increasingly complex in character. With the development of rapidly solidified, powder metallurgy Al alloys for high-strength and high-temperature applications, the capabilities of these materials have been pushed significantly forward through recent R&D studies.[1-4] A technology which has not kept pace with these developments is the appropriate low-cost method for fabricating components from these alloys. Consequently, the advantages offered by these materials are being questioned, as the already expensive structural materials require even more expensive fabrication methods. The development of cost-effective processing technologies, such as superplastic forming, isothermal forging, and other types of hot-working operations, is therefore urgently needed to enhance the application of these new-generation alloys. These call for an improved understanding of processability and microstructural models for predicting optimal process conditions and process limits.

Among the recent work on processing of advanced alloys, e.g., Al/SiC and elevated temperature Al alloys, the work of Gegel et al is noteworthy.[5-7] By using a streamlined (cosine-shaped) die (as originally developed by Richmond[8,9] for minimizing center bursting problem in extrusion), Gegel et al have shown that Al alloys containing SiC whiskers could be safely extruded with little whisker damage. This is very useful for producing extrusions from complex materials through reduction of hydrostatic tension in the workpiece which can reduce damage. Gegel et al have also found different microstructural conditions produced within different processing regimes similar to deformation processing maps. While different regimes of behavior are predictable from their dynamic

material model based on compression tests, the microstructural development resulting from such processing and correlation are empirical in nature. Correlations are expected between compression tests as well as streamline die extrusion because both processes are axisymmetric. However, in two important industrial processes, rolling and sheet-metal forming (or superplastic sheet-metal forming), where the stress states are plane strain and biaxial tension, respectively, the microstructural correlations do not agree with axisymmetric processes.[9] Since the extent of shear deformation components varies widely between these processes, it is reasonable to expect entirely different processing windows ($\dot{\varepsilon}$,T, etc.) for these processes from those for extrusion of similar materials, and these will be explored in this work.

In connection with the development of different microstructures during extrusion, Gegel et al have been able to develop ultra-fine microstructures (subgrain structures) in the advanced Al alloys by a process of dynamic recrystallization by extruding these materials at a high strain rate and a high homologous temperature.[10] Although prior particle boundaries begin to disappear when extrusion is carried out under these conditions, a closer examination reveals faint outlines of continuous oxide film along these boundaries. Streamline die provides uniform shear which is ideal for minimizing whisker damage, but not suitable for dispersion of oxide stringers. To achieve some degree of oxide dispersion, streamline die requires a greater extrusion ratio than a shear face die, since the latter introduces intense inhomogeneous shear. For superplastic forming of the extruded material, fine subgrain structures produced via extrusion could undergo dynamic recrystallization; however, the oxide stringers can adversely influence superplasticity by causing excessive cavitation. Since superplastic sheet forming processes develop more severe tensile conditions at the oxide stringers (causing cavitation) than does isothermal forging or extrusion, overall reductions of roughly 30:1 (extrusion plus thermomechanical processing) involving shear deformation are necessary to sufficiently disperse oxides in the billet.

Improved processability in the new, complex Al alloys could be achieved by 1) development of a very fine microstructure (subgrain and/or grain structure), and 2) developing new grain boundaries with simultaneous removal of prior particle boundaries (for P/M) or prior ingot structure boundaries (for I/M). The latter takes advantage of precipitation effects available in Al alloy systems, while the former depends, among other things, on the volume fraction and size of dispersoids usually present in Al alloys.

The alloys of interest for the present study are 1) an Al/SiC composite; 2) a second-generation, high-strength P/M Al alloy made by the rapid solidification method; and 3) a high-temperature P/M Al alloy produced via the rapid solidification method. The Al/SiC composites do offer an excellent combination of strength and elastic modulus; however, fracture toughness and fabricability are important considerations. The high-strength P/M alloy will be used in strength-critical areas where Al-Li alloys cannot be used, and high-temperature Al alloys (Al-Fe-Ce, Al-Fe-Mo, etc.) will be used in areas where temperature requirements are higher, but Ti is underutilized. Because of the pivotal role these alloys are likely to play in aircraft structures in the near future, cost-effective fabrication and processing technologies, such as superplastic forming and hot-forming techniques, must be found. It is also important that such processing does not deteriorate the service properties of the alloys.

A common method of microstructural refinement is static recrystallization of a deformed (rolled) alloy. This uses recrystallization of an alloy which has undergone significant amounts of cold work. Recently, it was found that when ultra-fine dispersoid particles are present (such as Al_3Zr and perhaps $FeAl_3$ and $FeAl_6$), the Zener pinning force exerted on the grain boundaries could be large enough to prevent grain boundary migration and full recrystallization of the alloy. The deformed structure, which primarily consists of subgrains, does exhibit some growth at higher temperatures, but does not form high angle boundaries. When aided by concurrent deformation, these boundaries can become mobile and sweep through other areas to increase misorientation between grain boundaries (continuous dynamic recrystallization). Evidence exists that fine equiaxed subgrain structures could form when the proper combination of extrusion and rolling deformation is used. The efficiency of this substructure formation could be significantly influenced by simultaneous precipitation effects present in Al alloys (since these precipitates can additionally pin the dislocations introduced), and therefore the process temperature may be critical.

3.2.2 Objectives

In the second year of this program, the objective for Part I is to develop a unified approach for deformation and thermomechanical processing of complex Al alloys. Specifically, selected alloys are to be subjected to three-axis plane strain forging and other deformation modes. Characterization of microstructural and crystallographic

texture changes, as well as their impact on elevated temperature flow characteristics, are to be documented.

3.2.3 Progress

Progress has been made in the following areas:

1. Both 7064 Al/15% SiC (particulate composite) and Al-Fe-Ce high-temperature alloy were subjected to large deformation strain via a repeated three-axis forging process.

2. The materials deformed by this process were examined by metallographic and pole figure (texture) analysis to ascertain the degree of concurrent recovery or recrystallization.

3. Characterization of tensile behavior of the processed material at elevated temperature has been carried out to assess the deformation mechanism and optimizing the processing window.

3.2.3.1 Materials Selection

The materials selected for the study on microstructural control included a material with heterogeneous microstructure such as a high-strength Al alloy reinforced with SiC particulate reinforcement. An alloy that was previously determined to have a significant potential for high strength and toughness, rapidly solidified PM-64 (7064) alloy, developed by Kaiser Aluminum Co., was selected as the matrix for this particulate composite. Composites were fabricated by blending 15 v/o of 1200 mesh SiC particulates with PM-64 powder, hot-outgassing and hot-pressing, followed by extrusion in a rectangular die (18:1 extrusion ratio). For comparison purposes, a matrix alloy containing no SiC particles (i.e., unreinforced PM-64 alloy) was also selected as the second material and processed in an identical manner. Third, a high-temperature Al alloy, Al-8Fe-4Ce, developed by Alcoa under AFWL contract, was selected. This alloy has shown promise for use at service temperatures as high as 500°F and is a likely candidate material for next-generation aircraft. This material was procured both in extruded plate and rolled

sheet form. The chemical compositions of the materials studied in this report are given in Table 1.

3.2.3.2 Processing of 7064Al/SiC

Inert gas-atomized powder 7064 Al (previous designation, PM-64) with SiC particulates is consolidated and extruded by Kaiser Aluminum Co. Kaiser uses a depurative outgassing technique which produces the final material with extermely low oxide content. The extruded plates (1 in. thick) were processed by a variety fo methods, which include reversed torsion, thermal cycling under compression, three-axis forging, followed by pancake forging and rolling. Figure 1 shows microstructures of 7064 Al/15% Sic material after three-axis forging to high levels of cumulative strain. (This is a repeated plane strain forging process which does not permit an overall change in specimen size, but allows the accumulation of a high level of strain.) The samples deformed by reversed torsion and thermal cycling were examined during last year's studies, and therefore studies were conducted on three-axis forged specimens in this part.

Table 1

Chemical Compositions (weight percent) of Advanced Al Alloys for Part I

Alloy Designation	Zn	Mg	Cu	Zr	Cr	Co	SiC	Fe	Ce	Al
1. PM-64 or 7064	7.2	2.4	2.0	0.2	0.12	0.2	--	< .05	--	Rem.
2. PM-64/SiC	7.2	2.4	2.0	0.2	0.12	0.2	15*	< .05	--	Rem.
3. CU78	--	--	--	--	--	--	--	8.0	4.0	Rem

* volume percent

Samples were examined for crystallographic texture in the following conditions: extruded; three-axis and pancake forged; and rolled after the forging step. Both (111) and (200) x-ray pole figures were developed. Figures 2, 3 and 4 show the (200) pole figure of this material in the three conditions discussed above. In Fig. 2, the direction of extrusion is normal to the plane of illustration. LTD indicates long transverse direction, while STD indicates short transverse direction. The predominant texture in this pole figure is analyzed and found to be (110) <111>, which is a typical hot-rolled texture for

SC41741

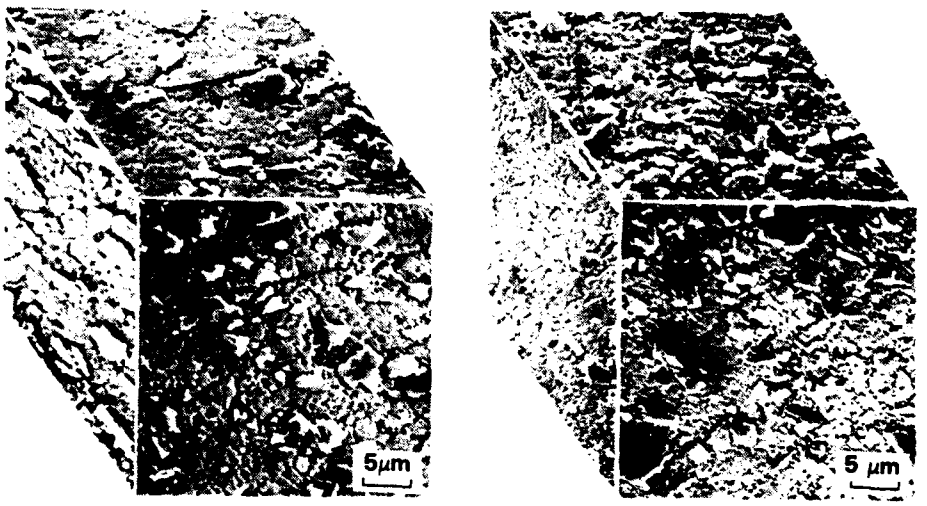

3-AXIS FORGING STRAIN ~ 6.9
G. SIZE ~ 3.2 μm

3-AXIS FORGING STRAIN ~ 12.4
G. SIZE ~ 1.7 μm

Fig. 1 Microstructure of 7064 Al reinforced with 15 v/o SiC particulates after three-axis forging to two different levels of cumulative strain.

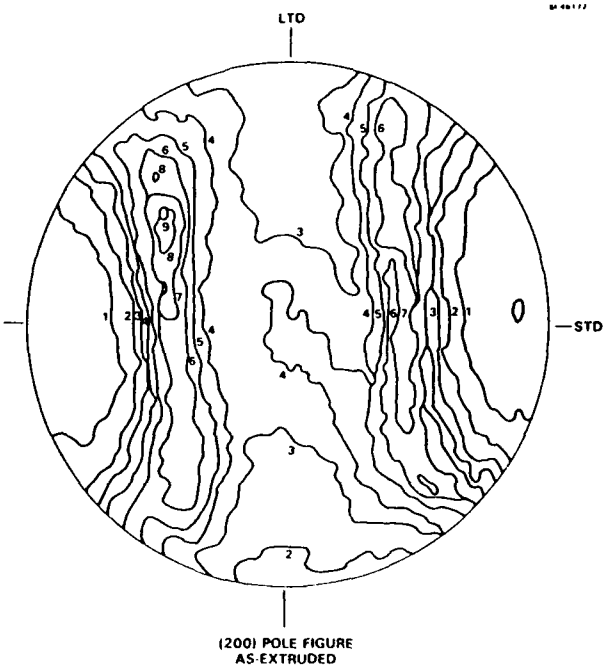

Fig. 2 (200) x-ray pole figure of as-extruded 7064 Al/SiC on a plane normal to the extrusion direction.

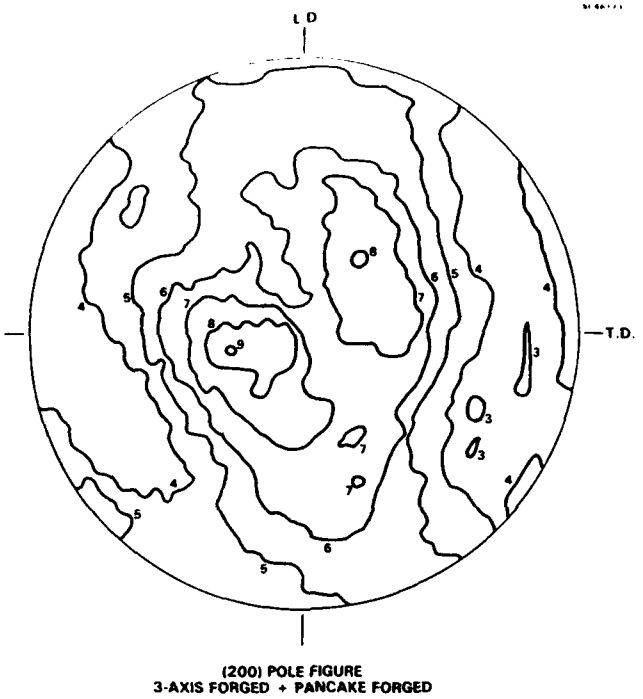

(200) POLE FIGURE
3-AXIS FORGED + PANCAKE FORGED

Fig. 3 (200) x-ray pole figure of three-axis forged and subsequently pancake-forged sheet of 7064 Al/SiC.

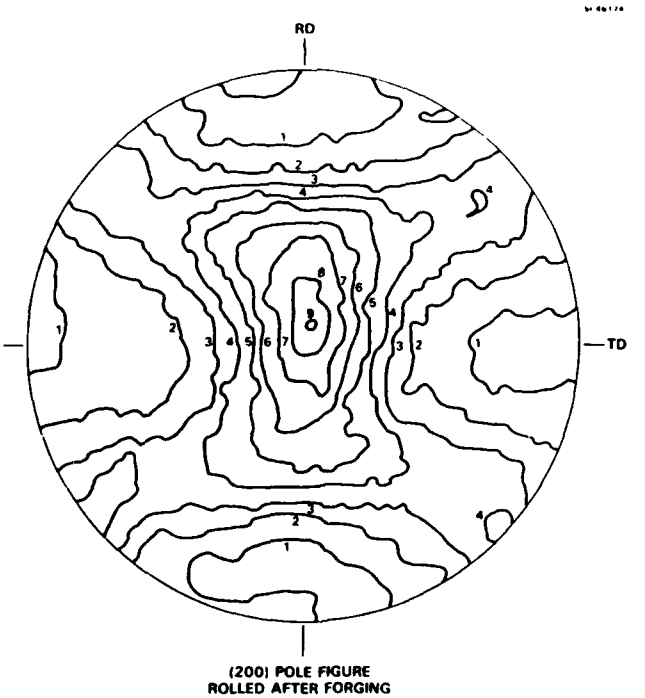

(200) POLE FIGURE
ROLLED AFTER FORGING

Fig. 4 (200) x-ray pole figure of forged and rolled sheet of 7064 Al/SiC.

Al alloys. Thus, the SiC particulates do not appear to hinder the appropriate texture formation. After three-axis forging, the block was flattened by pancake forging. At this stage (Fig. 3), the texture appears to be a combination of (200) $\langle 1\bar{2}\bar{2} \rangle$ texture with (310) $\langle 1\bar{3}\bar{3} \rangle$. These textures are a result of secondary textures upon breakup of (110) <111> recovered texture, which can happen due to shearing along several (111) slip planes, as expected during the three-axis forging process. Figure 4 shows a strong component of recrystallization texture in the forged and subsequently rolled material. This texture component is (100) <010>. Clearly, a microstructural destabilization process is operative to convert the recovered material into at least a partially recrystallized material.

Studies of elevated temperature deformation were carried out with materials both in as-rolled and further recrystallized states (480°C for 30 min followed by water quenching). The experiments were carried out in uniaxial tension at 450, 480 and 516°C at a variety of strain rates. Going up to higher temperature was found to cause the flow stress and strain hardening to decay and elongation to be lower. This trend was worse when the material did not have a final recrystallization step. It is believed that 7064 Al powder which was homogenized after atomization, consolidation and extrusion at a high enough temperature (480°C) develops a coarser dispersoid structure, and the material's ability to retain grain size and high elongation is lost. When a separate recrystallization treatment is given, the stability of the structure improves somewhat due to conversion of some of the low-angle grain boundaries into high-angle boundaries.

Figure 5 shows stress-strain curves for 7064 Al/SiC at 450 and 480°C. At a strain rate of 10^{-3} s^{-1}, the flow stress is reduced only 400 psi at 480°C; however, the strain hardening is sufficiently high to produce a respectable tensile elongation of 224%. At 450°C, however, the flow stress is higher and strain hardening is more rapid initially followed by a decay to lead to a lower level of elongation (15%). When strain rate is reduced, however, the rate of strain hardening drops and a lower elongation results, as shown by the bottom curve for $\dot{\varepsilon} = 2 \times 10^{-4}$ s^{-1}. Thus, the optimum processing conditions for these materials use a high temperature of 480°C with a relatively high strain rate of 10^{-3} s^{-1}.

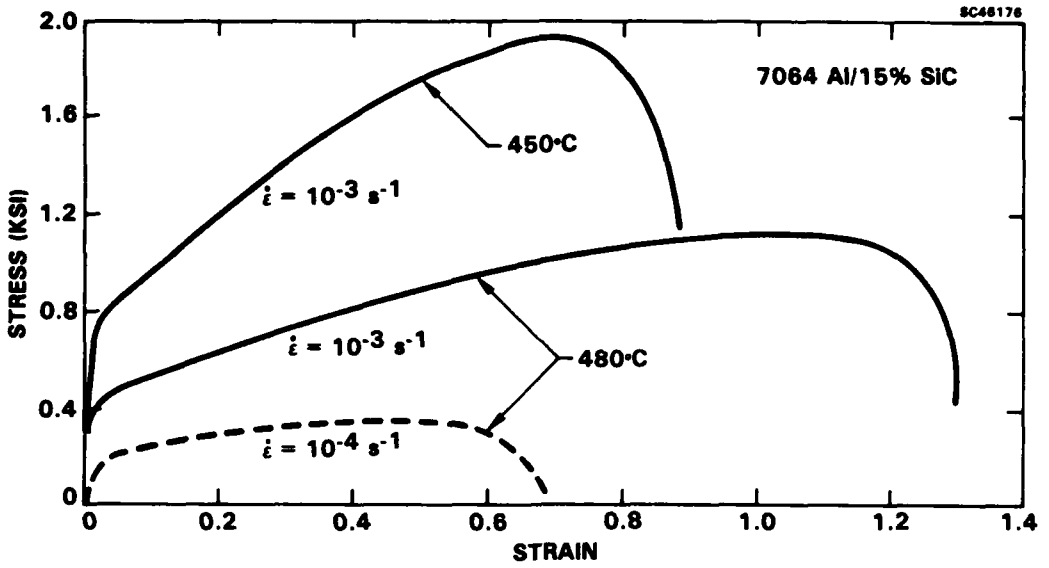

Fig. 5 Stress-strain curve for 7064 Al/SiC particulates for two different temperatures and strain rates.

3.2.3.3 Processing of High-Temperature Aluminum

Al-8Fe-4Ce alloy (CU78) atomized and powder-processed, subsequently consolidated and extruded by Alcoa was obtained in a 1 in. thick bar of rectangular cross section (1 in. x 4 in.). The extrusion ratio used was 9:1. Optical microscopy and SEM did not reveal the details of the extremely fine microstructure in this material. TEM was performed on thin foils prepared normal to the direction of extrusion. Figure 6 reveals the distribution of dispersoid particles in this material which shows both elongated and spherical (smaller) particles. The larger elongated particles were identified as $Al_{13}Fe_4$ and are typically 0.2-0.5 μm. The smaller particles were identified as $Al_{10}Fe_2Ce$ and are typically in the 0.05-0.1 μm range. Figure 7 shows a higher magnification of the same material showing the subgrains which are 0.05-1.2 μm. This micrograph also shows how the subgrain boundaries are well pinned by the various dispersoids, some of which are almost as large as the subgrains themselves.

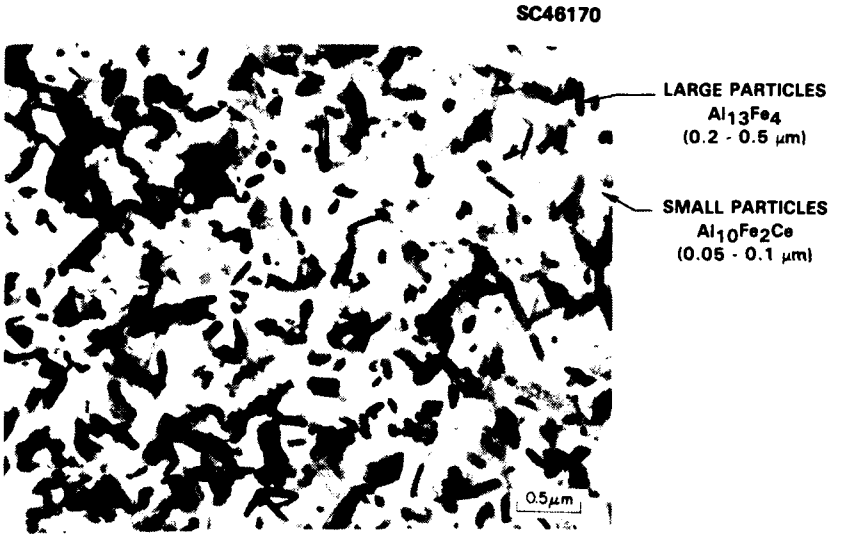

Fig. 6 TEM of CU78 alloy (Al-8Fe-4Ce) as extruded 9:1, viewed normal to the extrusion direction.

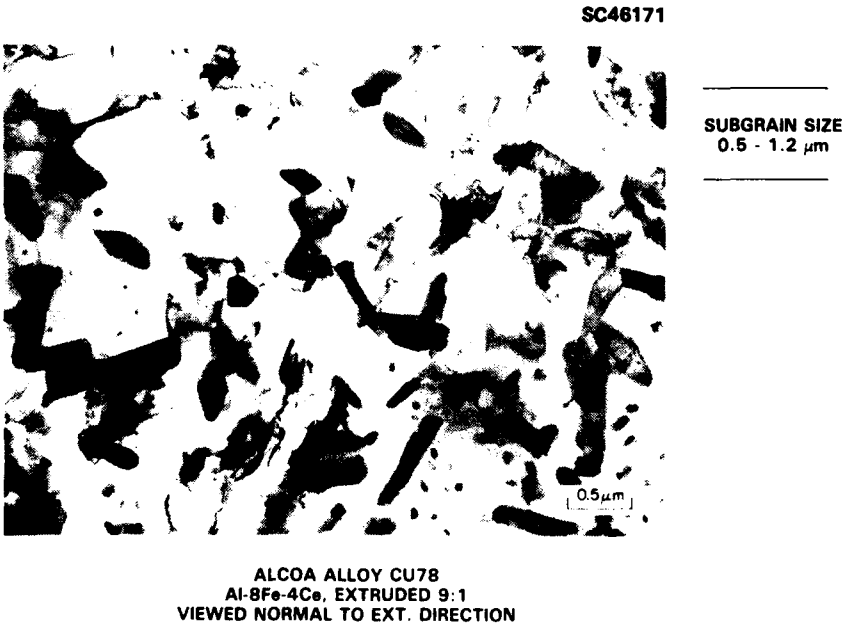

Fig. 7 TEM of CU78 alloy (as in Fig. 6) at higher magnification showing subgrain boundaries.

Elevated temperature tensile tests were carried out on the extruded material as well as samples which were three-axis forged and subsequently rolled. It was necessary to go as high as 520-530°C to develop extended ductility in this alloy. Figure 8 shows flow stress vs strain rate for this alloy in rolled conditions at 520°C. It appears that a high strain-rate sensitivity ($m = d\log\sigma/d\log\dot{\varepsilon}$) begins to occur as strain rate drops below $2 \times 10^{-5}\ s^{-1}$. However, since deformation times are very large, significant coarsening of the precipitates is expected at these strain rates. This subject will be investigated during the next reporting period. At strain rates around $10^{-3}\ s^{-1}$, the material exhibits dislocation creep behavior (with m values ~ 0.2) with flow stresses in the range of 200 psi or higher. The extruded material, when deformed in this condition, exhibits a tensile elongation of 55%. However, after three-axis forging and rolling, this elongation increases to 100%. While it is clear that the extruded microstructure is very

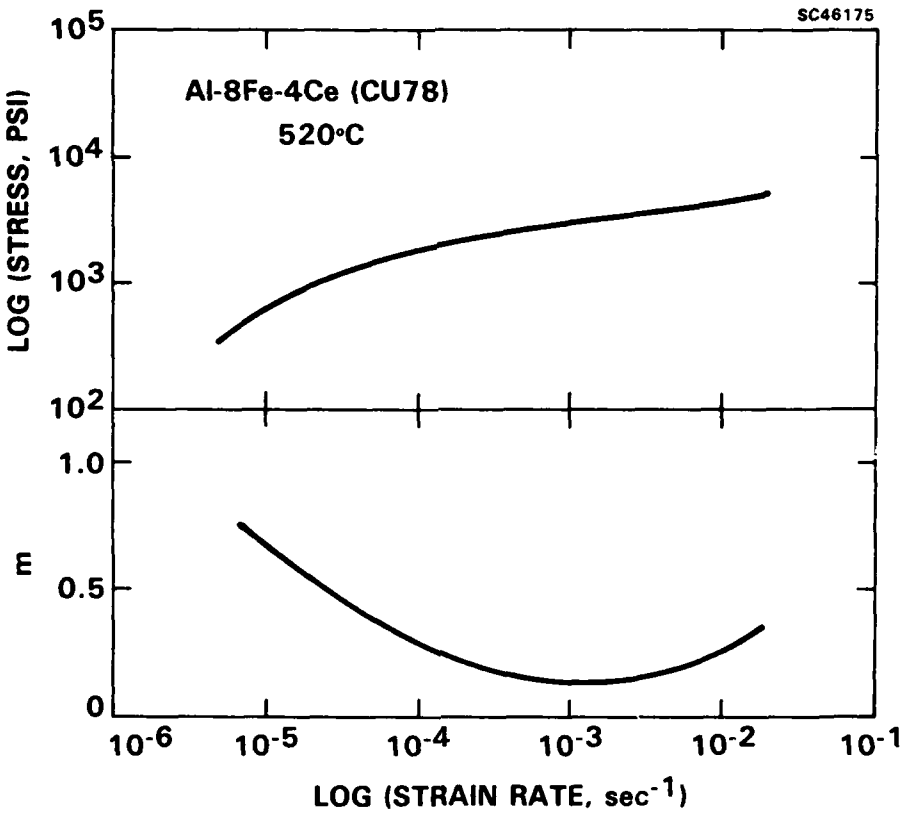

Fig. 8 Stress vs strain rate and m vs strain rate for CU78 in three-axis forged and rolled condition.

fine and additional thermomechanical processing does not further refine the microstructure, it is believed that further processing increases average misorientation ($\Delta\theta$) between subgrain, thereby enhancing subgrain diffusional creep, based on the model developed earlier in this program (Annual Report No. 1).

3.2.3.4 Summary

The deformation and thermomechanical processing characteristics of PM 7064 Al/SiC particulates and Al-8Fe-4Ce alloy have been studied by a number of deformation processing paths. X-ray pole figure analysis showed the conditions necessary for gradual development of a recovered texture, and subsequently a recrystallized texture. The recrystallized microstructure shows greater stability to processing conditions and increased tensile elongation at elevated temperature. The Al-8Fe-4Ce alloy shows two types of dispersoids (round - $Al_{10}Fe_2Ce$ and long - $Al_{13}Fe_4$) which pin the subgrain boundary structure to a very small size. The optimum processing temperature for 7064 Al/SiC was found to be 480°C and that for Al-8Fe-4Ce to be 520°C, while the forming strain rate was 10^{-3} s^{-1}. The best combinations of strain hardening and strain-rate sensitivity for PM 7064/SiC at 480°C and 10^{-3} s^{-1} produce a high ductility (tensile elongation = 224%).

3.3 Part II. Creep of High-Temperature Intermetallics

This section describes progress made in Part II during the second year of the three-year program to study creep behavior in Ti_3Al base alloys. The program goals are described, followed by a brief background outlining the basis of the program. Progress is then detailed.

3.3.1 Program Goals

The overall objectives of Part II of this three-year program are to:

1. Measure the effect of C, O, Si, Fe, Nb, V, Zr and Y on the 675°C creep resistance of Ti-23Al-8Nb (at%).

2. Evaluate the influence of the most effective additives listed above on the creep behavior of Ti-24Al-11Nb (at%).

3. Determine the mechanisms by which the minor alloying additions improve creep resistance in Ti-24Al-11Nb.

4. Assess the mechanisms by which primary creep strain contributes to total creep strain.

5. Determine the phenomenological description of creep in Ti aluminides and the influence of additives thereon.

3.3.2 Background

Creep strength in Ti alloys is generally defined, for design considerations, as the ability to withstand deformation up to some specific level, such as 0.1 or 0.2%, for a given time, temperature and stress level. Testing that is performed to qualify alloys within these types of guidelines will therefore include both primary and secondary creep deformation. The large scatter in data from qualification tests has been attributed to the variations in primary creep strain.[11] For instance, when Raut and Clough[12] could not get a good correlation of Ti creep-rupture data, they suggested it was due to "abundant scatter in the test results". Similarly, Bania[11] has shown that primary creep strain in Ti-6Al-2Sn-4Zr-6Mo varies in a manner that does not correlate with heat treatment. Rhodes' work on alpha + alpha two (alpha two = Ti_3Al) alloys has shown that alloys with identical secondary creep rates can have vastly different primary creep rates.[13] All of these results indicate that primary creep behavior in Ti alloys is not well understood.

The influence on creep behavior of minor additives to near-alpha and super-alpha Ti alloys has been documented over the last several years.[14-16] However, their effects on Ti aluminide alloys have not been investigated. Because of the differences in deformation characteristics between the disordered alpha phase of the near-alpha alloys and the ordered alpha-two phase of the Ti aluminides, it is not clear if the effects of these minor additives will be similar in the the two types of alloy systems. This program examines those effects.

The overall goal of this research is to improve the creep resistance of high-temperature Ti alloys. The specific objectives are to: 1) investigate the influence of C, O, Si, Fe, V, Nb, Zr and Y on creep resistance of Ti-22Al-8Nb (at%); 2) evaluate the contribution of primary creep to total creep strain; and 3) determine the mechanism by which the additives improve creep resistance. The effort in Part II is divided into two phases which will be performed sequentially. Phase 1 consists of a screening approach to evaluate the effects of eight different additives that have been shown to have a significant effect on properties of leaner Ti alloys. Tensile and creep tests at 675°C will provide sufficient information to determine which of the additives have the most significant effect on the creep resistance of the Ti aluminide base composition.

Phase 2 consists of a detailed study of the mechanism by which the minor alloying additives improve creep resistance in the base alloy. In addition, the mechanism by which primary creep strain contributes in total creep strain will be assessed by the use of transmission electron microscopy (TEM) of interrupted creep test specimens. These detailed studies will concentrate on the two alloy additives that most significantly influence creep strength as determined by the Phase 1 screening tests.

3.3.3 Summary of Previous Phase I Progress

It was reported in Annual Report No. 1 that creep tests at 675°C and 30 ksi revealed small variations in steady-state creep rates with small composition variations.[17] It was shown that creep rates could be reduced by reducing the concentration of Fe, O, or Nb, or by increasing the level of C, Si, or Si + Zr. Vanadium was found not to influence creep behavior under these test conditions.

During the current reporting period, further analyses have been performed on selected Phase I test specimens, the results of which are reported herein. Compositions of the Phase I alloys studied are listed in Table 2, where they are grouped by minor alloying additions (underlined). Alloy numbers correspond to those listed in Table 3 of Annual Report No. 1.

Table 2
Compositions of Ti Aluminide Alloys (at%)

Alloy	Ti	Al	Nb	Fe	O	C	Si	Zr
1	Bal.	23.5	8.54	.017	.251	.148	.010	.002
2	Bal.	23.3	8.28	.031	.253	.136	.007	.002
13	Bal.	23.0	8.34	.063	.280	.152	.088	.003
5	Bal.	23.2	8.39	.055	.298	.047	.105	.001
6	Bal.	23.6	8.98	.056	.281	.090	.100	.003
23	Bal.	22.8	8.29	.051	.341	.225	.085	.009
11	Bal.	23.7	8.59	.055	.298	.155	.095	.003
7	Bal	22.1	9.26	.061	.313	.154	.098	.002
9	Bal.	23.2	8.49	.060	.315	.155	.183	.001
19	Bal.	22.2	8.01	.052	.333	.136	.172	.298

Creep behavior at 675°C for the ten alloys is recapped in Table 3. The creep tests were conducted at 30 ksi constant stress which is about 40% of the yield strengths. All tests were carried through to fracture.

3.3.4 Fractography of Creep Test Specimens

All creep test specimens fractured primarily in mixed intergranular and transgranular modes with intergranular being dominant, Fig. 9. Gauge sections, however, exhibited varying surface crack patterns. For instance, some specimens cracked circumferentially around the gauge section along residual machining (grinding) marks, while others had only grain boundary cracks at the surface, Fig. 10 and Table 4. In general, those with circumferential cracks tended to have lower steady-state creep rates and primary creep strain (although Alloys 19 and 23 are exceptions). Furthermore, time spent in primary creep also correlates with the type of surface cracking: longer times correspond to circumferential cracks and shorter times correspond to cracks along prior beta grain boundaries. This observation indicates that those alloys with no grain boundary cracks

Table 3

Steady-State Creep Rates and Primary Creep Strains for Titanium Aluminides Tested at 675°C and 30 ksi

Alloy No.	Steady-State Creep Rate hr^{-1}	Primary Strain (%)	Time to Reach Steady State (h)	Composition Variant (at.%)
1	0.026	1.316	28.7	0.017 Fe
2	0.041	1.084	14.9	0.031 Fe
13	0.072	0.915	7.2	0.063 Fe
5	0.081	0.869	6.2	0.047 C
6	0.056	1.02	10.4	0.090 C
23	0.055	1.04	10.2	0.225 C
11	0.132	0.906	4.4	0.095 Si
7	0.098	0.933	6.1	0.098 Si
9	0.065	1.218	10.3	0.183 Si
19	0.042	0.900	10.7	0.047 Si+Zr

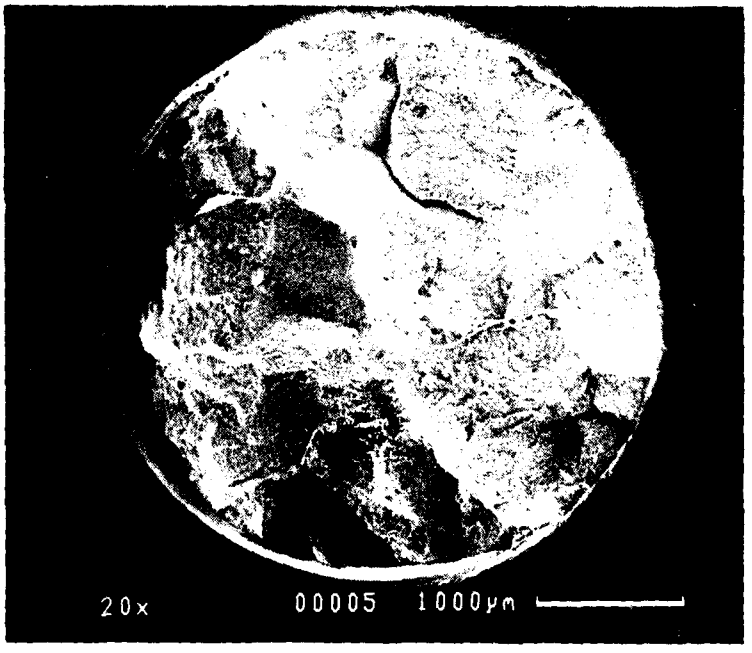

Fig. 9 Fracture surface of Alloy 1 creep tested at 675°C showing mixed fracture modes.

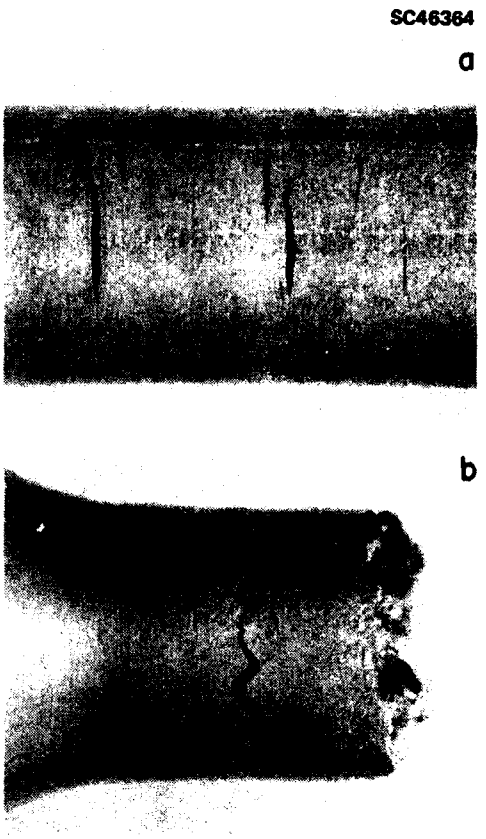

Fig. 10 Surface-cracking patterns on specimens creep tested at 675°C: (a) circumferential cracks in Alloy 2; (b) grain boundary cracks in Alloy 13.

Table 4

Surface Cracking Type in Creep-Tested Specimens

Alloy No.	Steady-State Creep Rate (h^{-1})	Time to Reach Steady State (h)	Surface Cracking Type
1	0.026	28.7	None
2	0.041	14.9	Circumferential
19	0.048	10.7	Grain boundary
23	0.055	10.2	Grain boundary
6	0.056	10.4	Circumferential
9	0.065	10.3	Circumferential
13	0.072	7.2	Grain boundary
5	0.081	6.1	Grain boundary
7	0.098	6.1	Grain boundary
11	0.132	4.4	Grain boundary

exposed on the gauge section surfaces have greater creep resistance than those in which grain boundary cracking has developed throughout the gauge section. Surface cracking, i.e., grain boundary vs circumferential, can then be interpreted as a measure of creep resistance.

3.3.5 Correlation of Minor Alloying Addition with Creep Behavior

Table 1 reveals that Alloys 13 and 11 have virtually identical compositions, yet secondary creep rates vary from 0.072 to 0.132/h. Fracture characteristics and surface-cracking patterns were observed to be the same for these two specimens, leading to the conclusion that the spread from 0.072 to 0.132/h represents experimental data scatter. Several of the creep tests fall within this scatter (i.e., Alloys 13, 5, 7, and 11) and others are close (i.e., Alloys 23, 6, and 9). It is a question as to whether all test results, except the very lowest (i.e., Alloys 1, 2, and 19) are within experimental error. We have concluded that the lower steady-state creep rates of Alloys 1, 2, 19, 23, 6, and 9 are outside experimental data scatter based on the following. As shown previously, steady-state creep rate, primary creep strain, and time spent in primary creep correlate in general with the test specimen surface-cracking patterns. Test specimens from Alloys 2, 6, and 9 exhibited circumferential surface cracks and each spent 10 h or more in primary creep. Test specimens from Alloys 13, 5, 11, and 7 exhibited only grain goundary surface cracks and each spent 7.2 h or less in primary creep. The general correlation suggests that alloys exhibiting circumferential surface cracks spend longer times in primary creep and have lower secondary creep rates than those containing grain boundary surface cracks. Our conclusion is that, because the alloys rank in the same order using steady-state creep rate, time spent in primary creep, or surface-cracking pattern, the lower creep rates measured from Alloys 1, 2, 19, 23, 6, and 9 can be interpreted as outside the experimental data scatter. The influence of alloying additives can be evaluated based on the above.

3.3.5.1 Iron Effects

Comparing Alloys 1, 2, and 13, Fig. 11, reveals that lowering the Fe level from 0.063 at.% (0.07 wt%) to 0.017 at.% (0.02 wt%) results in significant reductions of the minimum creep rate and increasing time spent in primary creep. As a consequence of

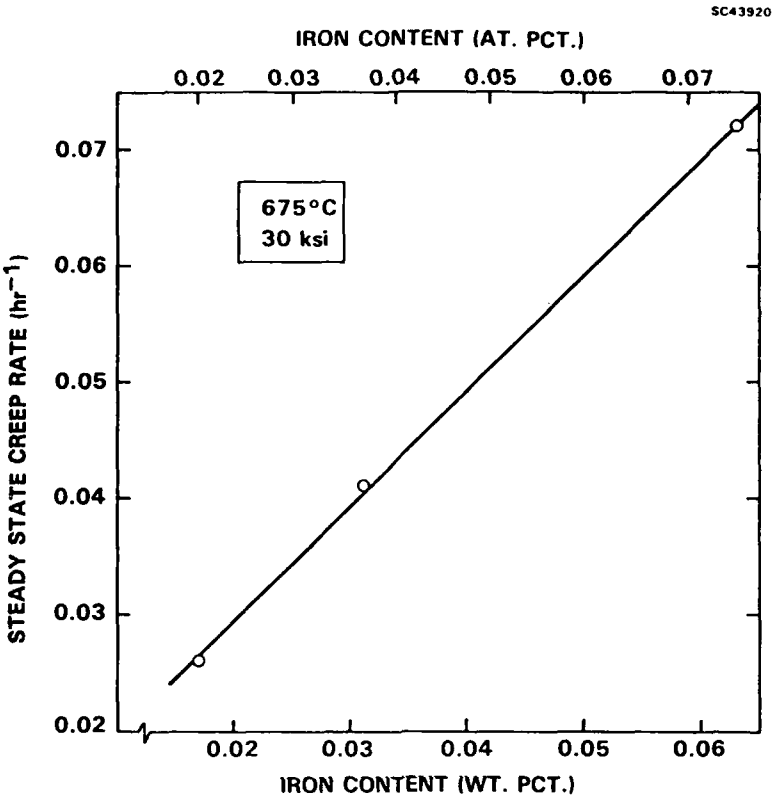

Fig. 11 Secondary creep rate as a function of Fe level in Alloys 1, 2, and 13. Tested at 675°C and 207 MPa.

these rate reductions, the time to reach 2% strain is raised from 20 h to 53 h. It is not realistic to suggest that Fe levels can be held to much below the 0.017 at.% of the alloys tested here, but it is clear that a minimum Fe level is desirable for creep resistance. In this sense, it can be concluded that Fe effects creep behavior of α_2 alloys in a manner similar to that observed for near-alpha and super-alpha creep-resistant alloys.[18]

Dislocation arrangements in creep specimens have been studied by thin-foil TEM. One mechanism for improving creep resistance would be an increase in the critical resolved shear stress required to activate all possible slip systems. If this were the case, one would expect to see fewer dislocations in the more creep-resistant alloy after any fixed time of creep exposure (i.e., less strain). In the Phase I creep tests, all specimens

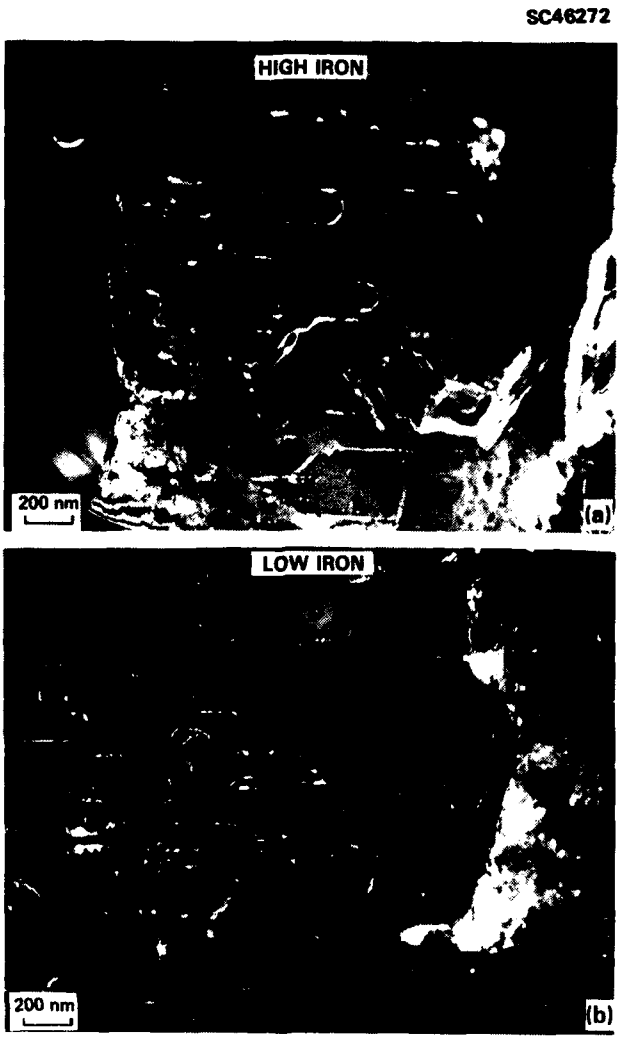

Fig. 12 Dark field TEM using [0002] reflecting vector to image c+a dislocations: (a) Alloy 13, high Fe; (b) Alloy 1, low Fe.

were tested to fracture, and so dislocation density is not a meaningful measure of deformation mechanism. Another mechanism for improving creep resistance would be an increase in the critical resolved stress of the non-a type dislocations, i.e., those with a c component in the Burgers vector. If this were the case, one might expect to see more c+a type dislocations in the less creep-resistant alloys. This difference would be present even in the specimens tested to fracture.

Dark field imaging with a [0002] g-vector reveals all dislocations that have a c component in their Burgers vector. By this technique, c+a slip dislocations can be observed without the tedious process of Burgers vector determinations. Dislocations in the low Fe and high Fe samples (Alloys 1 and 13) are shown in Fig. 12. There are slightly more c+a dislocations in the high Fe sample than in the low Fe sample, indicating that increasing the Fe content may lower the stress required to activate this type of dislocation. The results, however, are not yet conclusive, and will be investigated further in Phase II of this program.

3.3.5.2 Carbon Effects

Carbon has a positive effect on creep resistance, i.e., increasing carbon increases creep resistance, although the degree of its effect is less than the other elemental additions studied here, Fig. 13. Over a composition range of 0.047 to 0.225 at% (0.01 to 0.06 wt%) carbon, creep rates are reduced only a small amount. In super alpha Ti alloys, carbon is added to alter the microstructure by allowing heat treatments at temperatures closer to the beta transus.[19] Such was not the case here as Alloys 5, 6, and 23 each had basically the same microstructure. Because TEM has not been completed on these alloys, it can only be speculated that carbon provides a solid-solution strenthening effect in the α_2 alloys.

3.3.5.3 Silicon Effects

Si additions of about 0.10 at% (0.06 wt%) show the highest creep rates, and only in the alloy with 0.183 at% (0.11 wt%) is the creep rate reduced, Fig. 14. Paton and Mahoney[20] reported that 0.25-0.30 wt% Si was the optimum level for increasing creep resistance in near-alpha type alloys. Their conclusion was based on solubility limits for Si in the disordered alpha matrix, invoking a mechanism of silicide precipitation on mobile dislocations during creep deformation.

Unlike the Fe addition samples, the increased creep-resistant, high Si alloy exhibits a slight increase in c+a dislocation activity, Fig. 15. There is an indication in the TEM micrographs that dislocation pinning has occurred during creep deformation, as indicated by the arrows in Fig. 16. Although actual silicide particles could not be imaged, clustering of Si atoms on dislocations could be sufficient to inhibit their motion.

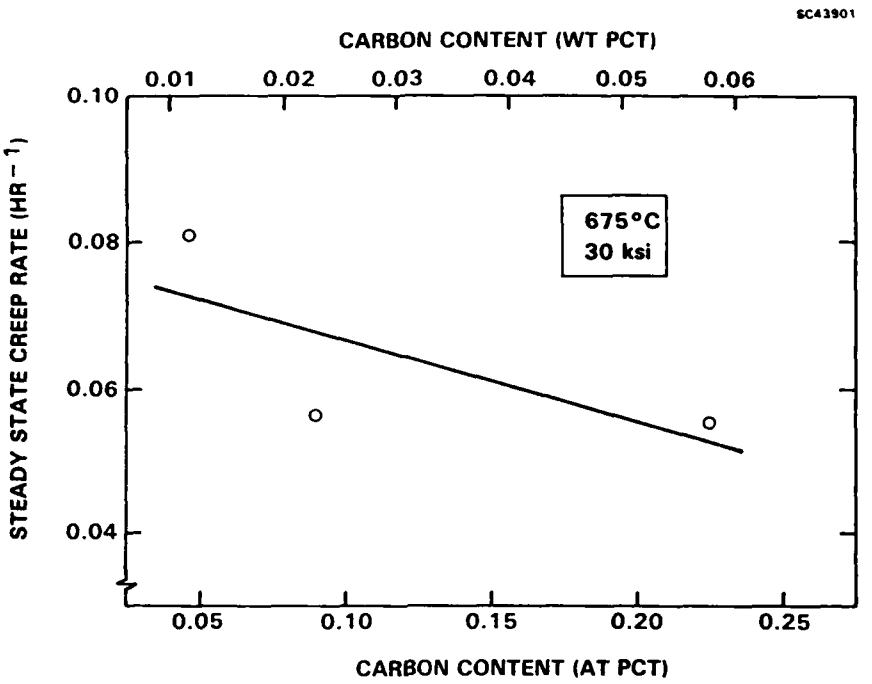

Fig. 13 Secondary creep rate as a function of carbon level in Alloys 5, 6, and 23. Tested at 675°C and 207 MPa.

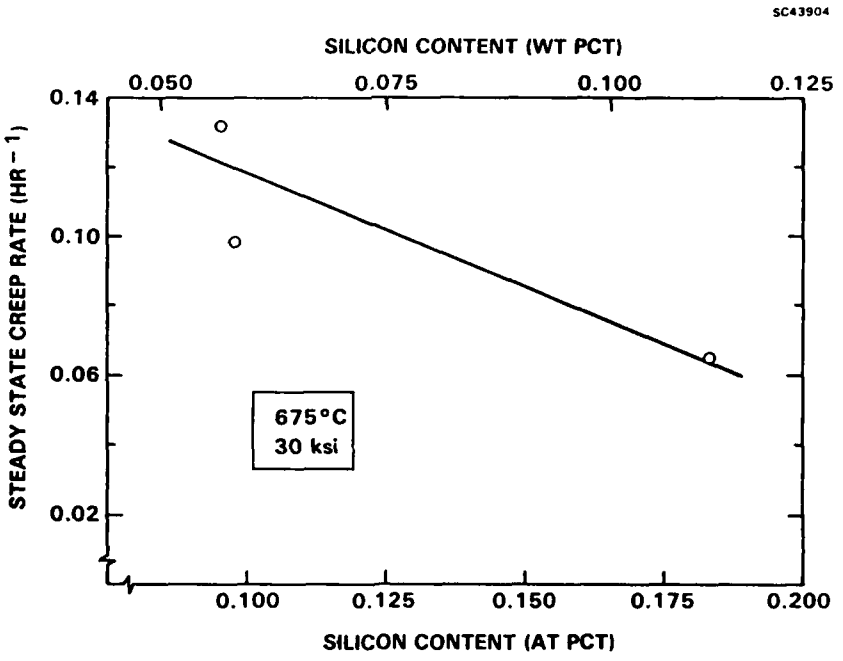

Fig. 14 Secondary creep rate as a function of Si level in Alloys 11, 7, and 9. Tested at 675°C and 207 MPa.

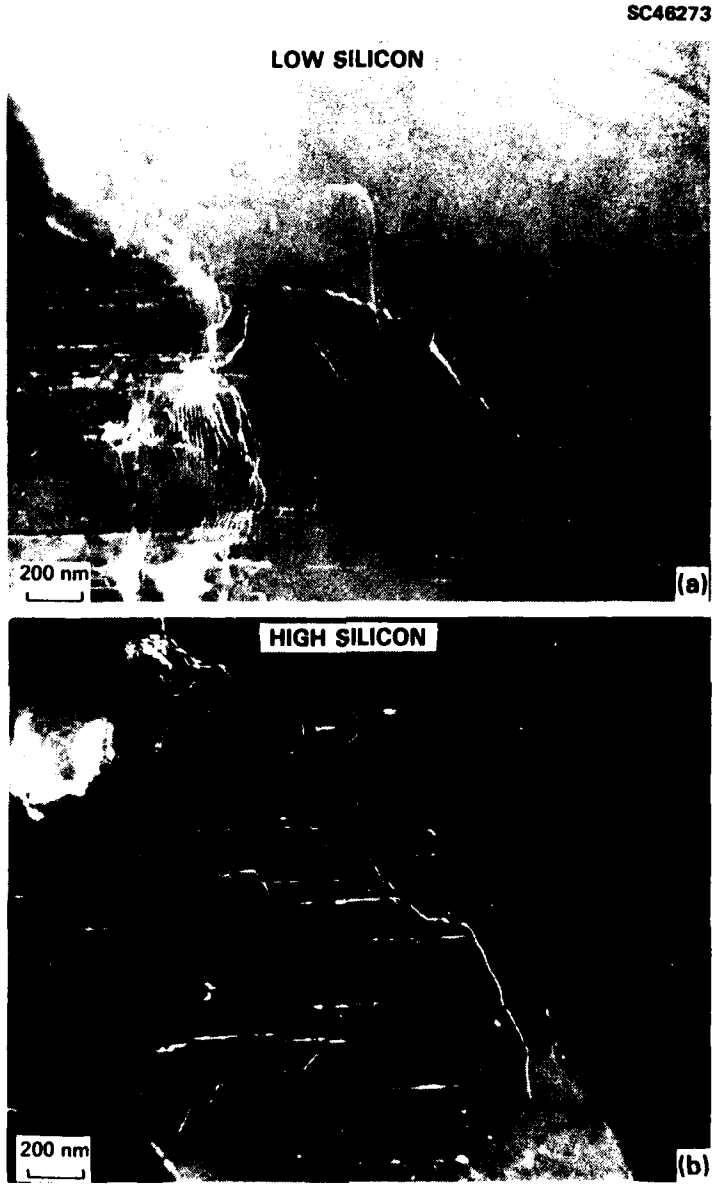

Fig. 15 Dark field TEM using [0002] reflecting vector to image c+a dislocations: (a) Alloy 11, low Si; (b) Alloy 9, high Si.

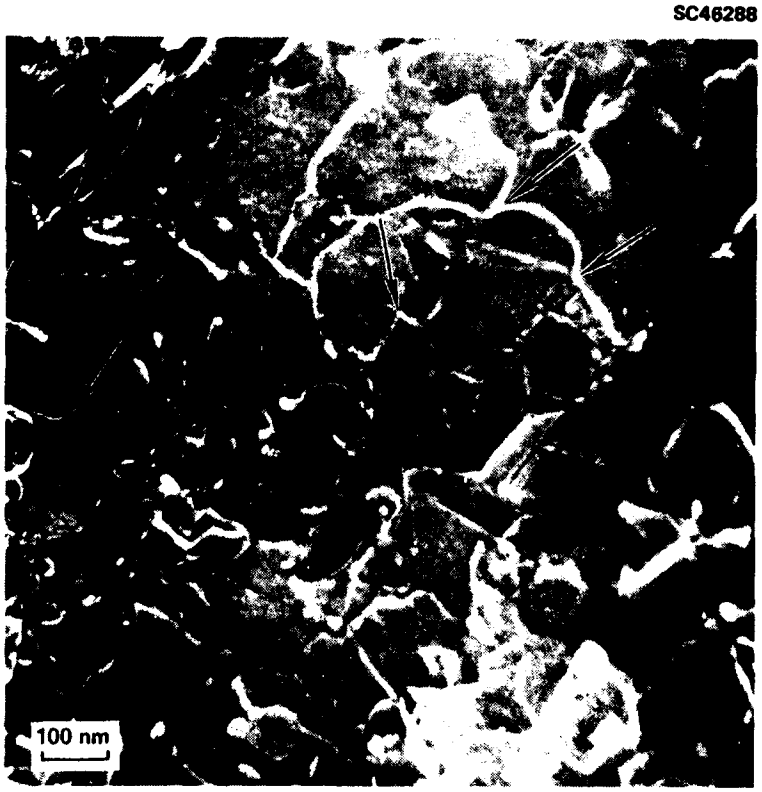

Fig. 16 TEM of creep-tested Alloy 9, illustrating pinned dislocations (arrows).

The Si levels examined here in the α_2 alloys are below the optimum value cited by Paton and Mahoney[20] for near-alpha alloys. However, the solubility limit for Si in α_2 + Nb alloys has not been determined. If the same mechanism holds for the α_2 structure, creep resistance would be expected to improve over that observed here with increased Si concentrations.

3.3.5.4 Silicon + Zirconium Effects

More effective in improving creep resistance than Si alone is the addition of Zr with Si, Fig. 17. A comparison of Alloys 9 and 19, which have virtually the same Si levels, reveals that the presence of Zr decreases the minimum creep rate. It has been suggested by others that Zr promotes a more homogeneous distribution of silicides,[21] and that mechanism likely holds for titanium aluminides.

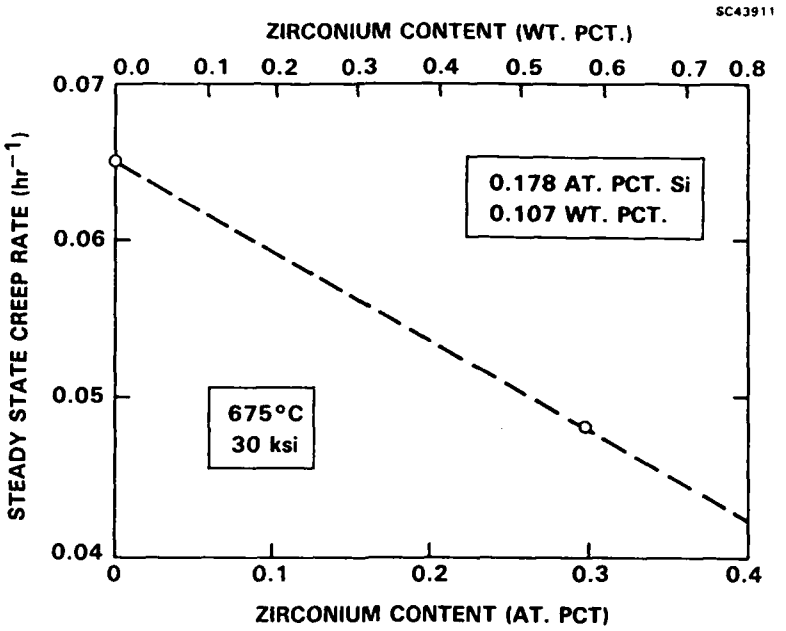

Fig. 17 Secondary creep rate as a function of Zr level in Alloys 9 and 19. Tested at 675°C and 207 MPa.

Comparing samples with and without Zr, Fig. 18, there appears to be a slight decrease in c+a dislocation activity with increased Zr. However, it is more likely that the mechanism of increased creep resistance is one of dislocation pinning. Figure 19 shows evidence of pinning of a-type dislocations that have been generated during creep deformation. There are more of these pinned dislocations in Alloy 19 (high Zr) than in Alloy 9 (low Zr).

3.3.5.5 Summary and Conclusions

The results have demonstrated that the effects of the individual additives on creep resistance at 675°C for the Ti_3Al base alloy are essentially the same as those previously observed for conventional Ti alloys. Si and Si + Zr are effective for improving creep resistance of the α_2 alloys by pinning mobile dislocations during creep exposure. Close control of Fe to its lowest possible level is also an effective approach to increased creep resistance. Carbon additions enhance creep resistance as well, although to a lesser extent than Si. Primary creep behavior as a function of alloying addition follows the same general trend as the minimum creep rate.

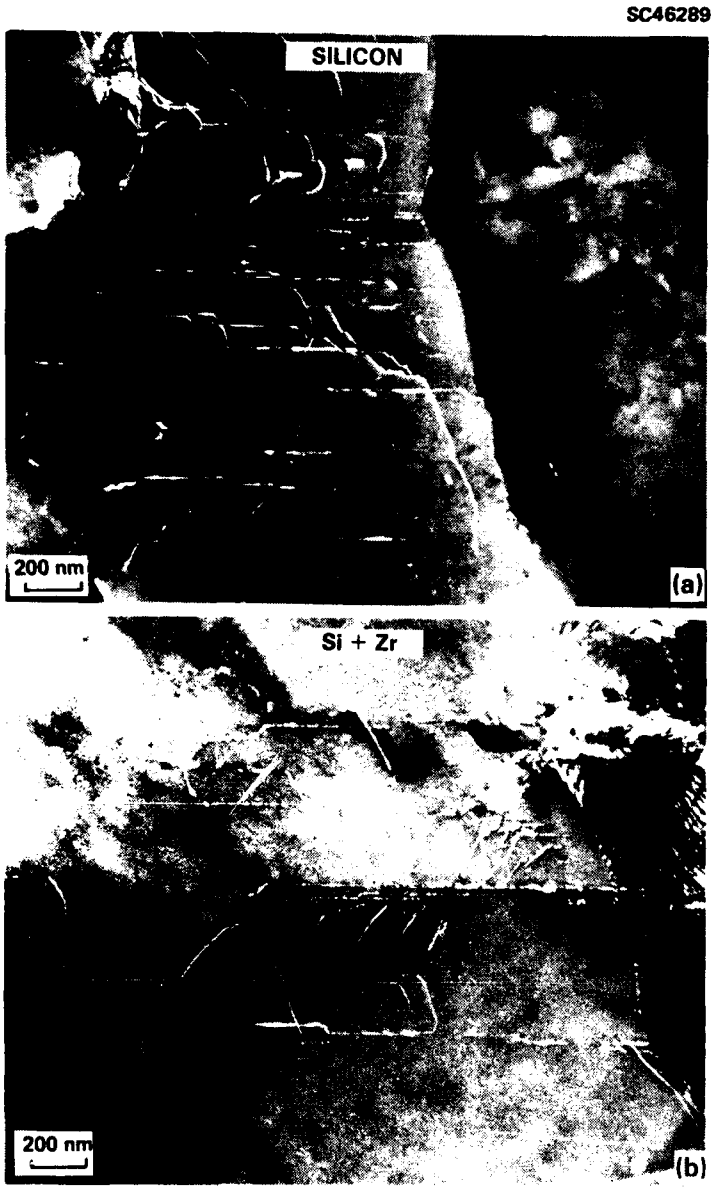

Fig. 18 Dark field TEM using [00022] reflection vector to image c+a dislocations: (a) Alloy 9, no Zr; (b) Alloy 19, high Zr.

SC46290

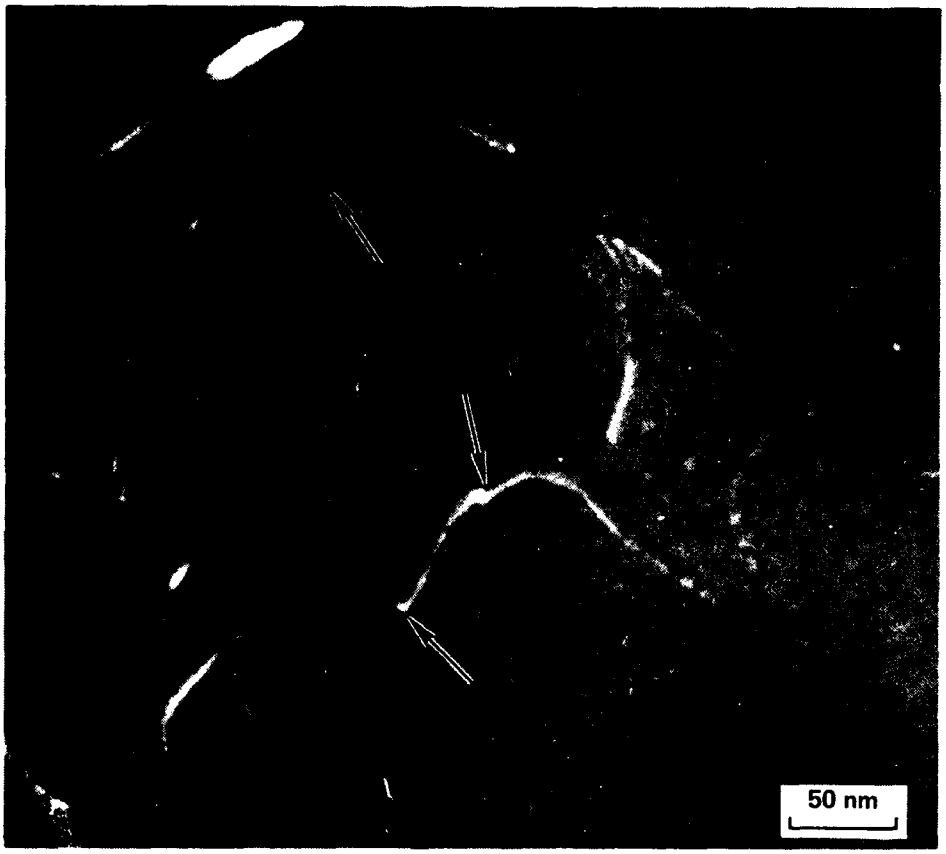

Fig. 19 TEM of creep-tested Alloy 19 illustrating pinned dislocation.

4.0 REFERENCES

1. M.E. Fine and E.A. Starke, "Rapidly Solidified Powder Aluminum Alloys," ASTM STP 890 (1986).
2. V. Anand, A.J. Kaufman and N.J. Grant, "Rapid Solidification of a Modified 7075 Aluminum Alloy by Ultrasonic Gas Atomization," Rapid Solidification Processing - Principles and Technologies II, Ed., R. Mehrabian, B.H. Kear and M. Cohen, Claitors Pub. Div., Baton Rouge, LA (1980), pp. 273-286.
3. C.M. Adam, R.G. Bourdeau and J.W. Broch, AFWAL Report, AFWAL-TR-81-4188, Feb. 1982, Contract No. F33615-76-C-5136.
4. R.E. Lewis, "Advanced Aluminum Alloy from Rapidly Solidified Powders," DARPA Order No. 3147, Report on AFWAL Contract No. F33615-78-C-5203.
5. Y.V.R.K. Prasad, H.L. Gegel, S.M. Doraivelu, J.C. Malus, J.T. Morgan, K.A. Lark and D.R. Barker, Met. Trans. A 15, 1883 91984).
6. J.S. Gunesekara, H.L. Gegal, J.C. Malas, S.M. Doraivelu and J.T. Morgan, Computer-Aided Process Modeling of Hot Forging and Extrusion of Aluminum Alloys (1984).
7. H.L. Gegel, J.S. Gunasekara, S.M. Doraivelu, J.C. Malas, J.T. Morgan and L.E. Matson, Consolidation and Forming of P/M Porous Billets (1985).
8. O. Richmond and M.L. Devenpeck, Proc. 4th U.S. Nat. Cong. of Applied Mechanics, 1503 (1962).
9. W.A. Backofen, Deformation Processing, Addison-Wesley Pub. Co. (1972).
10. J.P. Hirth and J. Lothe, Theory of Dislocations, McGraw Hill (1968).
11. P.J. Bania and J.A. Hall, "Titanium Science and Technology," Proc. 5th Int. Conf. on Titanium, G. Lutjering, U. Zwicker and W. Bunk, efs., Deutsche Gesellschaft fur Metallkunde E.V., Oberursel, 1985, pp. 2371-2378.
12. P.K. Kaut and W.R. Clough, "Titanium Science and Technology," Proc. 2nd Int. Conf. on Titanium, R.I. Jaffee and H.M. Burte, eds., Plenum Press, NY, 1973, pp. 2243-2254.
13. C.G. Rhodes, Rockwell International Science Center, Thousand Oaks, CA, unpublished research.

14. M.W. Mahoney and N.E. Paton, "The Effect of Minor Alloying Element Additions on Mechanical Properties of Titanium Alloys," Technical Report AFML-TR-77-56, May 1977.
15. G.S. Hall, S.R. Seagle and H.B. Bomberger, "Titanium Science and Technology," Proc. 2nd Int. Conf. on Titanium, R.I. Jaffee and H.M. Burte, eds., Plenum Press, NY, 1973, pp. 2141-2150.
16. M. Kehoe and R.W. Broomfield, ibid., pp. 2167-2178.
17. A.K. Ghosh and C.G. Rhodes, "Processability and High-Temperature Behavior of Emerging Aerospace Alloys," Annual Report, Contract No. F49620-86-C-0058, SC5459.AR, August 1987.
18. S. Ankem and S.R. Seagle, Titanium, Science and Technology, Proc. 5th Int. Conf. on Titanium, G. Lutjering, U. Zwicker and W. Bunk, eds., Deutsche Gesellschaft fur Metallkunde E.V., Oberursel, 1985, pp. 2411-2418.
19. D.F. Neal, ibid, pp. 2419-2424.
20. N.E. Paton and M.W. Mahoney, Met. Trans. A 7A, 1685-1692 (1976).
21. H.M. Flower, P.R. Swann and D.R.F. West, Met. Trans. 2, 3289-3297 (1971).

5.0 PUBLICATIONS AND PRESENTATIONS

1. A.K. Ghosh, "Deformation Processing of Al/SiC Composites at Elevated Temperatures," presented at the AIME Northeastern Chapter Symposium on High Temperature Composites, Stevens Institute of Technology, May 1987.
2. A.K. Ghosh, Microstructural Control and Processability of Advanced Aluminum Alloys," ONR Conf. on Materials Processing, Hyderabad, India, January 1988.
3. C.G. Rhodes, "Effect of Minor Alloying Additions on Creep Behavior of Ti_3Al + Nb," presented at 6th Int. Conf. on Titanium, Cannes, France, June 1988; and to be published in the Conf. Proc.
4. C.G. Rhodes, "Effect of Fe and Si on Creep Behavior of Ti_3Al + Nb," to be submitted to Met. Trans.

6.0 PERSONNEL ASSOCIATED WITH RESEARCH

Part I

Amit K. Ghosh, Principal Investigator
Leslie Holmes
Michael Calabrese
Fred Neveraz

Part II

Cecil G. Rhodes, Principal Investigator
Robert A. Spurling
Michael Calabrese
Peter Q. Sauers